applied sciences

MDPI

Article

Rapid Sonochemically-Assisted Synthesis of Highly Stable Gold Nanoparticles as Computed Tomography Contrast Agents

Mohammed Ali Dheyab [1,2,*], Azlan Abdul Aziz [1,2,*], Mahmood S. Jameel [1,2], Pegah Moradi Khaniabadi [2,3] and Ammar A. Oglat [4]

1 Nano-Biotechnology Research and Innovation (NanoBRI), Institute for Research in Molecular Medicine (INFORMM), Universiti Sains Malaysia, Pulau Pinang 11800, Malaysia; mahmood@student.usm.my
2 Nano-Optoelectronics Research and Technology Lab (NORLab), School of Physics, Universiti Sains Malaysia, Pulau Pinang 11800, Malaysia; p.khaniabadi@squ.edu.om
3 Department of Radiology and Molecular Imaging, College of Medicine and Health Science, Sultan Qaboos University, PO. Box 35, Al Khod, Muscat 123, Oman
4 Department of Medical Imaging, Faculty of Applied Medical Science, The Hashemite University, Zarqa 13133, Jordan; ammara@hu.edu.jo
* Correspondence: mohammed@student.usm.my (M.A.D.); lan@usm.my (A.A.A.)

Received: 15 August 2020; Accepted: 6 October 2020; Published: 9 October 2020

Featured Application: One of the applications of AuNPs in nanomedicine is treating cancer cells by Hyperthermia. Therefore, we suggest a future in vivo and in vitro studies to confirm the potential of AuNPs as a promising candidate for medical applications.

Abstract: One of the most widely used modalities of clinical imaging is computed tomography (CT). Recent reports of new contrast agents toward CT imaging have been numerous. The production of gold nanoparticles (AuNPs) as contrast agents for CT is primarily a topic of intense interest. AuNPs have beneficial features for this application, including excellent X-ray attenuation, flexible sizes and shapes, tailorable surface chemistry, excellent biocompatibility and high levels of contrast generating matter. AuNPs with a size of about 18.5 nm and semi-spherical shape were synthesized using a sonochemical method. The attenuation rate of X-rays as measured in Hounsfield units per unit concentration (HU/mg) was measured. Ultrasound treatment for a duration of five min has been shown to produce highly stable AuNPs in different media (AuNPs in water and phosphate-buffered saline (PBS) was −42.1 mV and −39.5 mV, respectively). The CT value (HU = 395) of the AuNPs increased linearly with an increase in the AuNP dosage. The results confirm the use of ultrasonic treatment for the production of metal nanostructures, particularly highly stable non-toxic AuNPs, with good morphology and high-quality crystal structure using an easy and fast method. Synthesized AuNPs have the potential to be used as a CT contrast agent in medical imaging applications.

Keywords: sonochemical method; AuNPs; zeta potential; highly stable

1. Introduction

Computed tomography (CT) is a common clinical presentation imaging technique that uses an X-ray source as well as an array of detectors to produce images [1,2]. CT has the ability to generate images with high spatial and temporal resolution [3]. CT offers three dimensional (3D) anatomical information on certain organs and tissues, including lung, liver, cardiovascular system and gastrointestinal tract, as a non-invasive diagnostic instrument [4]. Nevertheless, compared to the other

clinical imaging techniques, such as magnetic resonance imaging (MRI) and nuclear imaging, the lack of CT sensitivity to contrast agents is a major drawback [5]. Consequently, biomedical researchers are spending considerable efforts in developing a novel CT contrast agent.

Gold nanoparticles (AuNPs) have attracted increased attention due to their distinctive and exceptional physicochemical features, such as electrical conductivity, low toxicity, high absorption spectrum, photothermal effects, adjustable size and shape-dependent optical properties, biocompatibility, chemical stability and easy functionality, relevant to a wide range of applications in biomedicine, catalysis, material science and quantum dots technology [6–12]. The usefulness of the nanoparticles colloids for biomedical application depends on their stability and biocompatibility of the nanoparticles in solution [13]. Since nanoparticles are transported through cavities, canals, waterways and aquifers [14], their stability in aqueous systems is vital to the formulation of predictive and transport models [15]. In addition, the toxicity of nanoparticles (NPs) has been shown to be dependent on their stability [16], which has also led to a need to understand the behavior of NP suspensions to be settled. Generally, the stability of NPs is influenced by their physical and chemical characteristics such as size [17], morphology, material composition [18], and surface coating [19]. Although several studies have been carried out on the sonochemical synthesis of AuNPs, none of them investigated the significant effect of their stability and their potential for CT [20–29].

Sonochemical synthesis is one of the most widely used methods for nanomaterial synthesis due to the critical features that can be generated from acoustic cavitation [30–32]. It involves the nucleation, expansion and collapse of microbubbles by propagating a pressure wave through a liquid. This involves the implosive collapse as well as subsequent release of massive energy at high pressure (1000 atm) and high temperatures (5000 K), which, in turn, produces shear forces, turbulence, microjets and shock waves [33]. It is a valuable instrument for escalating the mass transfer process at the surface and disrupting the adsorbent interface [34]. Nanomaterials can be produced and modified by utilizing ultrasonic irradiation to aid the synthesis process in aqueous solutions. The acoustic cavitation generated by ultrasonication in water provides transient bubbles in which the various physical and chemical phenomena produced by their implosion play a crucial role in the formation of nanostructures [35,36]. In addition, the sonochemical technique offers better control of the particle size/size distribution of NPs [37–39]. Different methodologies have been used to synthesize AuNPs. Piella et al., and Wang et al., reported that AuNPs had been successfully prepared using a reduction method with a reaction time of approximately 47 min and 90 min, respectively [40,41]. In another method, Dong et al., demonstrated that AuNPs were synthesized by reducing the number of gold ions with sodium borohydride by Turkevich for about 60 min [42]. Both methods mentioned above were laborious and time-consuming. Effectively synthesizing appropriate AuNPs via a simple and fast approach remains a challenge. On the basis of this claim and our previously published work, the sonochemical method can be considered as one suitable synthesis method to deliver stable AuNPs as a contrast agent for CT with a core diameter of approximately 20 nm in less than five min compared to 120 min required by the work of Ping et al. [43]. In addition, the application of the sonochemical method opens a window for researchers to investigate the reduction in the reaction time for nanoparticle synthesis [44].

In this work, a rapid and single-pot aqueous method of highly stable AuNPs achieved by the use of sodium citrate as a stabilizer and reducing agent is reported. In addition, the effect on cell viability is also studied to investigate cytotoxicity against HEK-293 in vitro and AuNPs as a potential contrast agent for CT. The NPs were subjected to ultrasonic treatment for the duration of five min to synthesize AuNPs with high stability and a mean size of 18.5 nm. The crystallinity/crystal structure, morphology, stability and absorption properties of synthesized gold NPs were obtained, analyzed and comprehensively discussed.

2. Materials and Methods

2.1. Characterization of AuNPs

X-ray diffraction (XRD) patterns of AuNPs were acquired at room temperature, utilizing an X-ray diffractometer (PANalyticalX'pert PRO MRD PW 3040, Enigma Business Park, UK) with CuKa (λ = 1.54050 Å) to investigate their crystalline structure. The size of the sample was derived using transmission electron microscopy (TEM, Zeiss Libra 120, Oerzen, Germany) at 100 kV. The ImageJ software (1.52 v) was used to measure the particle size distribution of the sample from approximately 50 particles. The absorption properties of the AuNPs were determined using ultraviolet–visible (Uv-vis) spectrophotometry (UV-3600, Shimadzu, Santa Clara, US). The stability, polydispersity index (PDI) and hydrodynamic size of the AuNPs were measured using a dynamic light scattering (DLS) instrument (ZETASIZER Nanoseries Model ZEN 3600, Malvern Instruments, Enigma Business Park, UK).

2.2. Materials

The following chemicals including sodium citrate ($Na_3C_6H_5O_7$), agarose gel XP, phosphate-buffered saline (PBS) and chloroauric acid ($HAuCl_4{\cdot}4H_2O$) are the precursor chemicals utilized for the synthesis. They were bought from Sigma-Aldrich. All chemicals were directly utilized without additional purification.

For cell culture, cell proliferation reagents (WST-1 assay) were purchased from Sigma-Aldrich. Human embryonic kidney 293 cells (HEK-293) were acquired from the American Type Culture Collection (United States of America (USA)). Fetal bovine serum (FBS), Dulbecco's modified Eagle's medium (DMEM), trypsin–ethylenediamine tetraacetic acid, penicillin, and streptomycin were purchased from Capricorn Scientific.

2.3. AuNPs Synthesis Using a Sonochemical Approach

Sonochemical synthesis involves the use of sound or sonic energy to excite particles, thereby initiating Brownian motion. The sonochemical technique can be used to efficiently disperse nanoparticles in fluids; therefore, it is regularly used in nanotechnology to facilitate homogeneous dispersion of NPs suspended in liquids. In addition, sonic energy can transform the chemical mechanism that controls the synthesis of the particles. The probe sonicator model (Vibra-Cell Ultrasonic Solid Horn) used for synthesis has a tip size, frequency and ultrasound output power of half-inch, 20 kHz and 17.9 W·cm^2, respectively. Precursor materials used to synthesize citrate-coated AuNPs include $HAuCl_4$, sodium citrate and distilled water. In order to prepare the sample, the first step involved the dissolution of $HAuCl_4$ in distilled water with a concentration of 0.03 M. Subsequently, the solution of $HAuCl_4$ (2 mL) was added dropwise to 20 mL of aqueous 0.03 M sodium citrate solution. During the mixing phase, a high-density ultrasonic probe (20 kHz) with an ultrasonic horn was inserted into the solution for 5 min at a sounding power of 17.9 W·cm^2. Ultrasound power has been determined using the underlying equation (Equation (1)) [45].

$$Power\ (\mathrm{W}) = Energy\ (\mathrm{J})/Time\ (\mathrm{s}) \quad (1)$$

where energy (J) and time (s) denote energy consumed (J) and duration of reaction, respectively.

Finally, in order to eliminate impurities and non-reactive particles, the AuNPs were centrifuged at 9000 rpm for 10 min and washed thoroughly twice using distilled water. Subsequently, the obtained particles were stored in two ways: (1) re-dispersed in distilled water for size, optical properties, stability and hydrodynamic size measurements; (2) some dispersion was dried for 24 h at 90 °C to obtain the powder for XRD, cytotoxicity and CT imaging measurements.

2.4. Cytocompatibility Experiment

Cytocompatibility of the citrate-coated AuNPs in terms of cell viability was examined by the WST-1 assay. Concisely, HEK-293 cells were exposed to standard culture in DMEM (containing 10%

of FBS, 1% *v/v* penicillin and streptomycin), which was pre-warmed in water baths maintained at 37 °C. After 24 h, cells were harvested using trypsin and afterwards re-suspended in fresh DMEM for seeding in 96-well plates (10^3 cells/well). Following cell attachment, different concentrations of AuNPs (0.1–0.5 mg/mL) in DMEM were added to cells then cells were incubated at 37 °C in a humidified environment of air (95%) and CO_2 (5%) for a different time; 24 h and 48 h. After incubation time, the cell proliferation reagent WST-1 was newly prepared at 10% in DMEM in the dark. The medium of each well was carefully removed and 10 µL of WST-1 solution plus 100 µL DMEM were added to each well. Following that, plates were returned into the incubator at 37 °C for 45 min to 2 h. Then, each well was read using a microplate reader (ELx800, BioTek Instruments, USA) at a primary wavelength of 480 nm. The percentage of cell viability was determined by the underlying equation (Equation (2)):

$$\text{cell viability (\%)} = (\text{OD Sample/OD control}) \times 100 \quad (2)$$

2.5. In Vitro CT Samples Preparation

The CT phantom was formulated from the agarose gel to determine the possibility of using AuNPs for CT imagery. The CT phantoms were prepared from agarose gel XP, via the dissolution of 1 g of agarose gel XP in 100 mL distilled water at 80 °C. Then, 1 mg of AuNPs (powder) was dispersed in 700 µL of distilled water and then 300 µL of agarose XP hot solution was added to the mixture in 2 mL vials. The same procedure has been followed for the other concentrations. Five gel phantoms containing different amounts (1, 2, 3, 4, and 5 mg/mL) of NPs were prepared plus a blank (control) agarose gel phantom. The samples were kept cool until they solidified. A Toshiba Aquilion LB (Model TSX-210A) CT scanner was used for the CT imaging. The brightness of the images denotes the intensity of the signal. The criteria for CT imaging include 80 kV X-ray voltage, and 100 mA anode current through the head window (W: 120 Hounsfield units (HU), L: 40 HU)). To determine HU values, the images were evaluated using the program MICRODICOM based on signal strength (Equation (3)). The image matrix, slice thickness and slice distance and field of view (FOV) were set at 320 mm, 3 mm, and 640/640 mm, respectively.

$$\text{HU} = 1000 \times ((\mu X - \mu\text{water}) / \mu\text{water}) \quad (3)$$

where HU = Hounsfield unit, X = tissue and µ = linear attenuation coefficient.

2.6. Statistical Analysis

The data were statistically evaluated using IBM SPSS (IBM SPSS Statistics for Windows, version 25.0., IBM Corp., NY, EUA). The results were recorded as geometric mean (%) ±STD. The differences among the independent groups were comparatively analyzed using Kruskal–Wallis and non-parametric Friedman tests. The Mann–Whitney test was utilized as the post hoc analysis. A level of 5% was considered statistically significant.

3. Results and Discussion

3.1. XRD Analysis

The XRD spectrum, as can be seen in Figure 1, proves the successful formation of AuNPs using sonochemical methods. All diffraction peaks fit perfectly into the face-centered cubic phase (fcc). The results of the XRD are in good agreement with the report of Geetha Bai et al. [46]. The characteristic diffraction peaks of (111), (200), (220), (311) and (222) are identified at 2θ values of 38.1°, 44.4°, 64.6°, 77.8°, and 81.6°, respectively, which are consistent with those in the reference (ref. code 01-089-3697). The XRD peaks are distinct because of their relatively high intensity. This finding can be attributed to the ultrasound's ability to control the process of crystallization through acoustic cavitation [47]. The sonochemical approach, therefore, provides better crystalline AuNPs as the XRD spectral characteristics (intensities and peak shifts) denote, comparing with other methods [48,49].

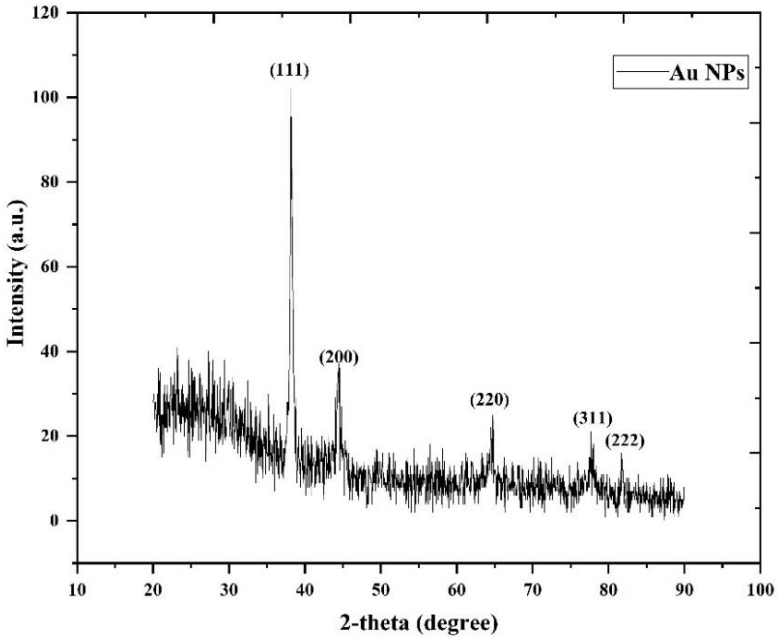

Figure 1. XRD pattern of face-centered cubic (fcc) structure gold nanoparticles (AuNPs).

3.2. TEM and Size Distribution

Transmission electron microscopy (TEM) image of the AuNPs is presented in Figure 2a. The TEM analysis was performed by placing one drop of the sonicated sample on the carbon-coated copper TEM grid and dried in air for 30 min. The core diameter of the AuNPs was 18.5 nm and semi-spherical [50] and almost uniformly-sized, as shown in Figure 2c. The addition of sodium citrate has made it possible to achieve the homogeneity in size and shape of AuNPs [51,52]. In addition, the uniformity of nanoparticles may also be related to the high energy and intense power flow generated by ultrasound irradiation during the formation and breakdown of bubbles, which increases the temperature and pressure of the solution. Morphological characterization of AuNPs reveals that the NPs are semi-spherically shaped with smooth geometry. The ultrasonic power is responsible for the formation and collapse of the bubbles, these bubbles produce hot spots, which have intense local temperatures (~5000 K) and pressures (~1000 atm), sometimes identified as a micro-reactors [53]. Moreover, the collapse of the bubble leads to an intense flow of power within the solution. The size of the nanoparticles is therefore formed under crucial conditions through ultrasonic power via the cavitation process.

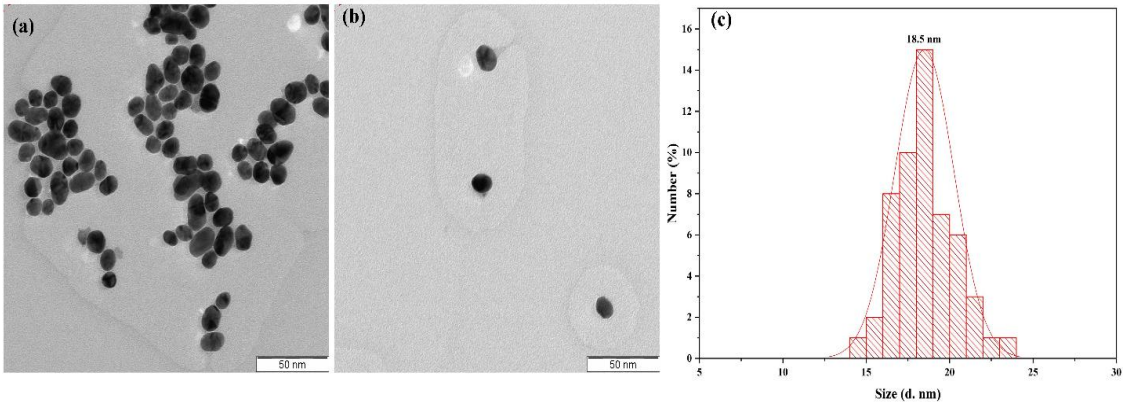

Figure 2. (**a**,**b**) (TEM) image with a scale of 50 nm and (**c**) size distribution of AuNPs synthesized at ultrasound output power 17.9 W·cm^2.

3.3. UV-Visible Analysis

Surface plasmon resonance (SPR) is an analytical technique used to describe changes in electronic configurations of NPs because of surface effects. Measurements of the SPR NPs band offered an indirect piece of evidence to substantiate the creation of AuNPs. The SPR was determined within 400–700 nm under ambient conditions using distilled water as the reference sample. The peaks of AuNP (SPR) can be adjusted from visible to infrared in the electromagnetic spectrum. The main characteristics of the SPR is a sharp decline with decreasing core size for AuNPs due to the onset of quantum size effects that become significant for particles with core sizes less than 3 nm in diameter. Thus, the SPR is absent for AuNPs with a core diameter of less than 2 nm, as well as for bulk gold [54]. AuNPs display the SPR band at about 520 nm in the visible region and the SPR band peaks and the wavelength is usually influenced by the particle size [55].

In this study, the suspensions of Au ions and AuNPs are shown in Figure 3. The final color of the suspension is shiny red, as can be seen in Figure 3c. The aqueous colloidal solution of Au was transformed from dark red to red at the start of ultrasonic treatment. After 5 min of sonication, the red shine color remained unchanged. The UV–vis spectral analysis of the AuNPs reveals a SPR absorption band at 520 nm (Figure 3a), which is consistent with the previous study [51,55].

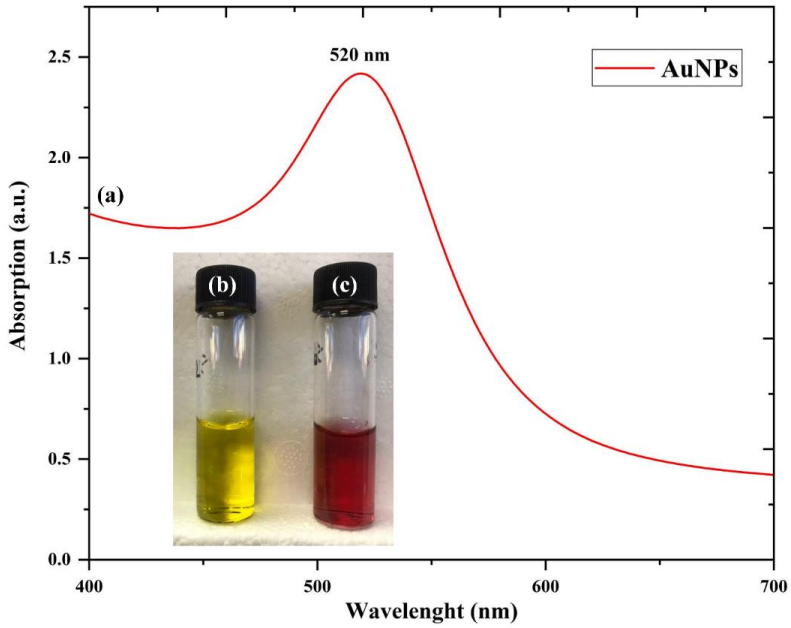

Figure 3. (**a**) Surface plasmon resonance (SPR) of AuNPs, which have a diameter of about 18.5 nm, (**b**) $HAuCl_4$ suspension and (**c**) AuNPs suspension.

3.4. Dynamic Light Scattering (DLS)

Zeta potential, polydispersity index (PDI) and hydrodynamic size have been measured using the dynamic light scatter (DLS) analysis. The PDI and zeta potential have been used to evaluate the stability of the as-synthesized AuNPs. Nanoparticles must be stable and homogeneously dispersed in biological media for biomedical applications [56]. The zeta potential values from 0 to ±5 mV indicate rapid agglomeration and suspension precipitation, ±10 to ±30 mV are incipient to instability, ±30 to ±40 mV denote moderate stability, while ±40 to ±60 mV denote good suspension stability [57,58].

The stability of metal particles in colloidal suspensions depends on the presence of electrical surface charges. In the case of AuNPs obtained sonochemically, the use of sodium citrate increases the stability of the colloids by acting as both a stabilizer and a reducing agent that hinders aggregation. Sodium citrate activates the reaction of Au ions with carboxylate ions ($–COO^-$), resulting in the reduction of the metal to Au^0.

AuNP formation takes into account the fact that free radical species are generated by ultrasonic irradiation for water molecules (Equation (4)). The reaction is expressed below.

$$\begin{array}{c} Na_3C_6H_5O_7 \xrightarrow{\text{Sonic} \gg\gg} Na_2C_5H_4O_5 + CO_2 + Na^+ + H^+ + 2e \\ Au^+ + 2e \rightarrow Au^0 \end{array} \quad (4)$$

The stoichiometry of the reduction reaction can be described as; the high energy of the ultrasonic ray helps to break the ion bonds of sodium citrate, releasing a pair of free electrons. These charge carriers reduce the golden ions that are suspended in the aqueous solution creating more Au^0 atoms. Figure 4 shows that the colloidal stability of AuNPs in water and PBS was −42.1 mV and −39.5 mV, respectively, indicating that the colloidal suspension of nanoparticles is highly stable. The negative sign of the zeta potential is attributed to adsorbed negative ions such as hydroxide anions (OH−) derived from the aqueous medium [56]. This negative charge can be attributed to the absorption of citrate onto the surface of Au [40]. These high negative values of zeta potential for AuNPs confirmed the presence of negatively charged carboxylate groups on the surface of the nanoparticles. A repulsion force between suspended particles is caused by zeta potential, which increases with the increase in surface charge of the particles suspended in the solution [50]. The sonochemical method can be a valuable tool for the preparation of AuNPs because the high energy generated by the radiation waves prevents cluster agglomeration and results in stable dispersion [59].

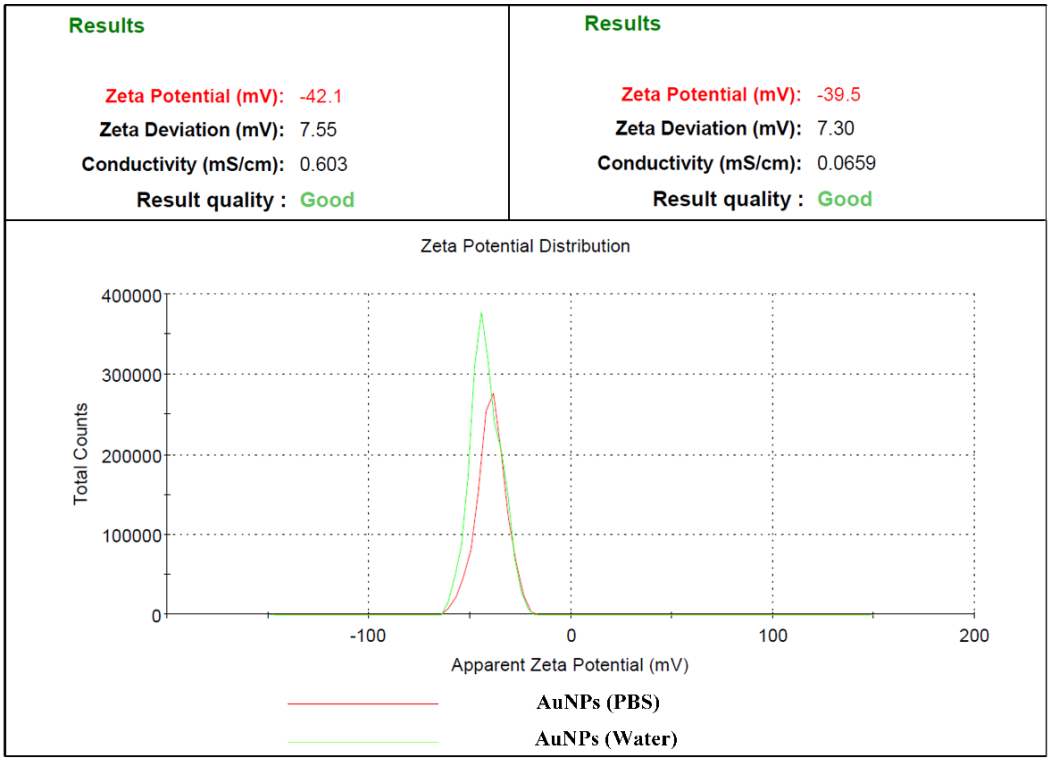

Figure 4. Zeta potential results of AuNPs suspension after 5 min of sonication. AuNPs dissolved in water (green solid line) and dissolved in phosphate-buffered saline (PBS) (red solid line).

As shown in Figure 5, the PDI values of AuNPs dissolved in water and PBS are 0.368 and 0.406, with a hydrodynamic size of 22.17 nm and 23.49 nm, respectively. Although there is a smaller second peak corresponding to the agglomeration, the emphasis here is on the first peak to evaluate the size of the particles and, for this reason, the agglomeration peak will be overlooked [60]. It should be noted that the difference in particle sizes between DLS and TEM is the result of larger particles scattering more light in the DLS technique, which moves the peaks towards the larger end of the size range, while

the TEM displays the true particle [61,62]. More specifically, this outcome may be attributed to the broad distribution of the mixture of the two particles.

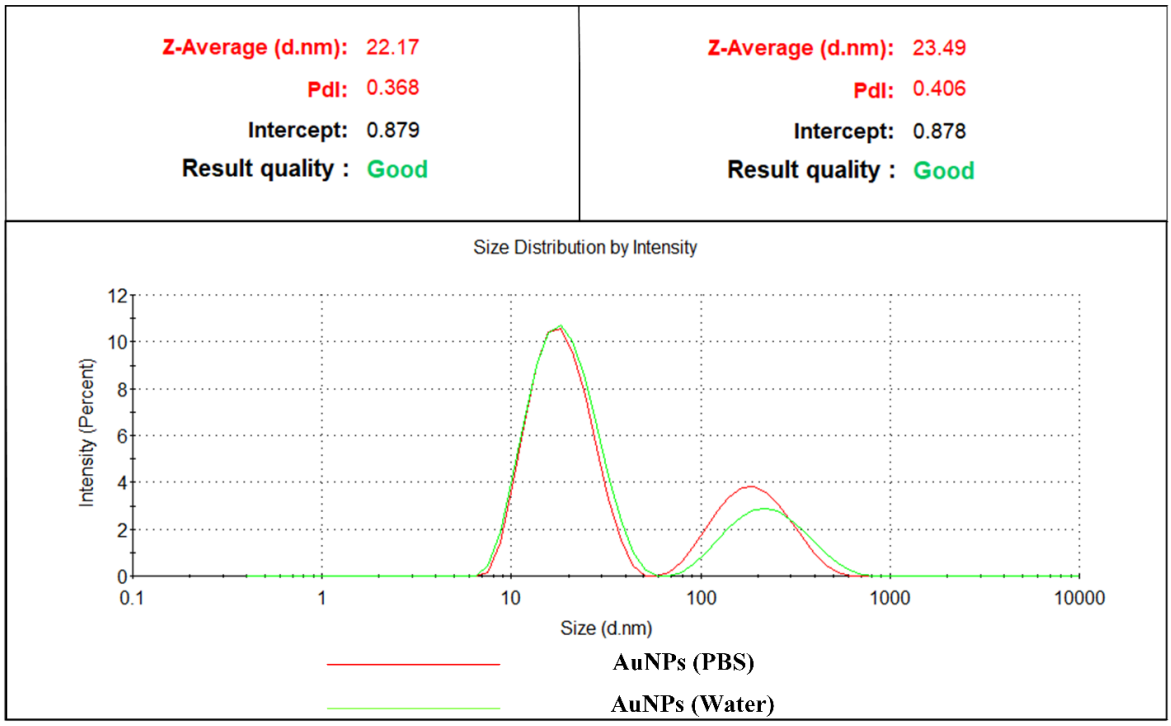

Figure 5. Polydispersity index (PDI) and hydrodynamic size of AuNPs prepared through sonochemical method. AuNPs dissolved in water (green solid line) and dissolved in PBS (red solid line).

3.5. Cytocompatibility Experiment

WST-1 based cytotoxicity study was performed on HEK-293 cells by incubating with AuNPs synthesized by a sonochemical approach in a range of concentration 0.1–0.5 mg/mL. In this study, human embryonic kidney cells were picked for two major reasons: (a) according to the previous studies, kidney is one of the organs, after spleen and liver, where AuNPs were accumulated as well as an excretion route [63]; (b) the cytotoxicity reaction may also be associated with the exposure concentration of the AuNPs. The type of cell has no impact on the cytotoxicity of the studies [64]. The results are presented in Figure 6. In the control group (HEK-293 cells without AuNPs) of all test replications, cell viability was defined at the constant rate of 100% with no fluctuations (zero standard deviation). The Mann–Whitney test results depict the mean cell viability values as significantly reduced at a concentration of 0.5 mg/mL after 24 h of incubation time at concentrations of 0.4 and 0.5 mg/mL after 48 h ($p < 0.01$). The Kruskal–Wallis test shows no significant differences between independent experimental groups for 24 h ($p = 0.176$) and 48 h ($p = 0.553$). A 10% to 20% reduction in the number of HEK-293 cells treated with 0.1–0.5 mg/mL AuNPs after incubation time (48 h) was observed in comparison to the 24 h incubation time. Despite that, as demonstrated in Figure 6, the percentage of cell prolonged was more than 70% at all concentrations and different treatment periods. The results of this study show that there were no cytotoxicity effects on HEK-293 cells at a range of concentration 0.1–0.5 mg/mL AuNP. Nanoparticles with cell viability above 70% have been reported to be suitable as biocompatible material [65]. Therefore, the synthesized AuNPs have the potential to be used as biocompatible diagnostic nanoprobes.

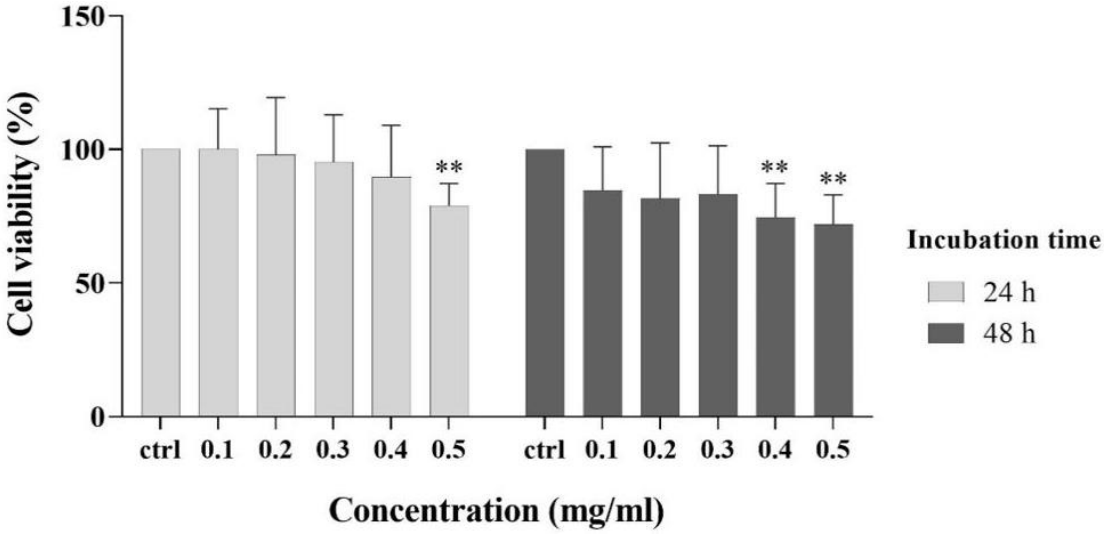

Figure 6. Cell viability using WST-1 assay. HEK-293 cells treated with specific concentrations of AuNPs (0.1–0.5 mg/mL) for 24 h and 48 h. An asterisk indicates a significant difference between the experimental groups and control (using Mann–Whitney test, ** p-value < 0.01).

3.6. In Vitro CT Imaging

The use of AuNPs as a CT contrast agent is much more appropriate due to enhanced X-ray attenuation compared to the standard CT iodine-based contrast agent [66]. In order to assess the ability to use AuNPs as a contrast agent for CT, different AuNP concentrations of X-ray attenuation have been tested using agar as a control sample (Figure 7). Images were analyzed directly by using the MICRODICOM (v3.3.2) program based on the signal strength of the HU values. The intensity of the CT image has been shown to increase with the increase in Au concentration. Figure 7 (inset) shows that the value of AuNPs CT (HU) increases linearly with an increase in the concentration of Au (HU = 395) [67]. CT imaging experiments show that the AuNPs produced have a higher attenuation strength than the clinically utilized iodine contrast agent, Omnipaque (a popular iodine-based CT contrast agent currently used in the clinic) [68], at the same molar concentration of active elements (Au or iodine) and activate significantly enhanced CT imaging. Figure 7 reveals that 2.3 mg Au/mL was equal to 7.2 mg/mL of iodine in Omnipaque (viz., 178 HU) in X-ray absorption. It leads to an X-ray attenuation nearly 3.1 times that of the iodine contrast agent, which may be due to the presence of electron-dense nanogold. The AuNPs have a higher atomic number as well as density (79 and 19.32 g/cm^3, respectively) relative to iodine (53 and 4.9 g/cm^3) leading to this effect [69]. Therefore, instead of conventional iodine-treated materials, such as barium sulfate or zirconium dioxide contrast agents, being used in CT, the toxicity of which is of major concern [70], we suggest the use of biocompatible nanomaterials produced via non-toxic methods, with high X-ray attenuation. The findings are consistent with a previous study [71]. Sun et al., indicated that ultrafine AuNPs had more X-ray attenuation than larger counterparts, likely because of their higher volume-to-surface ratio [72]. This is extremely important because the ability of AuNPs to attenuate X-rays is needed as a contrast agent for the potential use of CT images. The in vitro (HU) findings support the effectiveness of AuNPs in CT imaging. Overall, the influence of AuNPs on the X-ray attenuation of contrast CT imaging agent depends on the concentration of AuNPs.

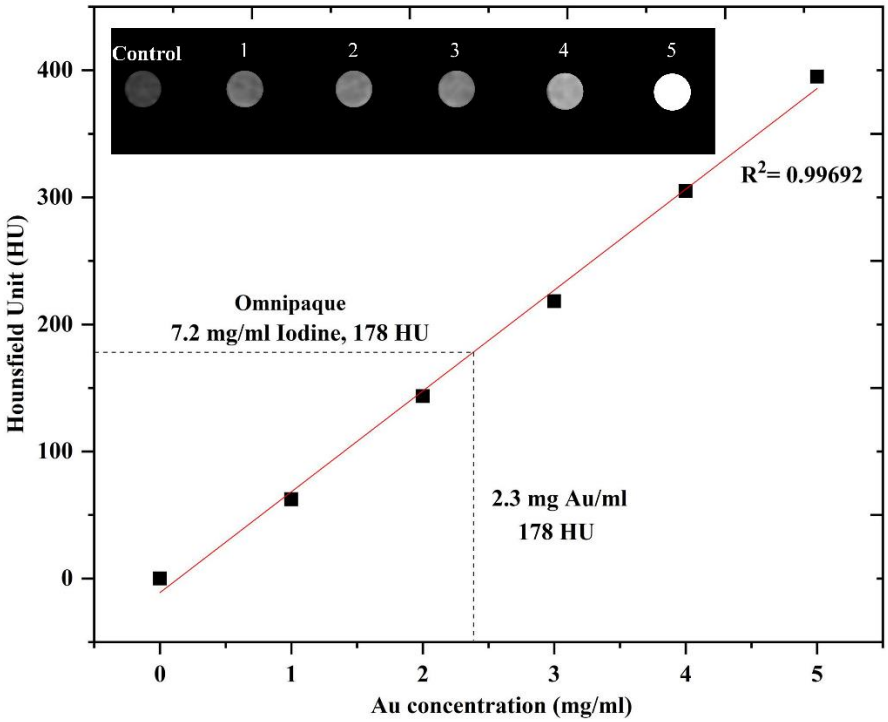

Figure 7. Computed tomography (CT) image of the AuNPs with different concentrations (1, 2, 3, 4 and 5 mg/mL) and X-ray attenuation intensity, the dotted line shows that 2.3 mg Au/mL gave an equivalent X-ray absorption as 7.2 mg/mL Iodine in Omnipaque (viz., 178 HU).

4. Conclusions

This study successfully synthesized AuNPs of 18.5 nm using a sonochemical approach and sodium citrate as a stabilizing and reducing agent. After five min of ultrasonic irradiation treatment, the citrate-coated AuNPs, dissolved in water and PBS, have the hydrodynamic size in aqueous suspension of about 22.17 nm and 23.49 nm with a PDI of 0.368 and 0.406, respectively. Sonochemical treatment also ensured that the colloidal suspension of nanoparticles was highly stable in different media (AuNPs in water and PBS was −42.1 mV and −39.5 mV, respectively). Due to their exceptional stability observed by zeta potential, AuNPs could also be used for various medical applications. The results confirm the use of ultrasonic treatment for the production of metal nanostructures, in particular non-toxic AuNPs, with a highly stable colloidal suspension and good morphology. In addition, a significantly enhanced CT value (HU = 395) show that AuNPs have the potential to be employed as a contrast CT agent in which their X-ray attenuation was linearly correlated with AuNP concentration.

Author Contributions: M.A.D., A.A.A. and M.S.J. conceived the idea and designed the experiments. A.A.A. supervised all the experiments and analyses. M.A.D., M.S.J. and P.M.K. prepared materials, performed characterizations, measurements and analyzed the results. A.A.A., P.M.K. and A.A.O. commented on manuscript writing. M.A.D. wrote the manuscript and all authors discussed the results and commented on the manuscript of the work. All authors have read and agreed to the published version of the manuscript.

Funding: This research was funded by Malaysia Ministry of Higher Education FRGS grant, grant number 203/PFIZIK/6711678. The APC was funded by Malaysia Ministry of Higher Education FRGS grant.

Acknowledgments: The authors would also like to thank School of Physics, Universiti Sains Malaysia for supporting this research work.

Conflicts of Interest: There are no conflicts of interest.

References

1. Hsieh, J. *Computed Tomography: Principles, Design, Artifacts, and Recent Advances*; SPIE Press: Washington, DC, USA, 2003.
2. Chhour, P.; Naha, P.C.; O'Neill, S.M.; Litt, H.I.; Reilly, M.P.; Ferrari, V.A.; Cormode, D.P. Labeling monocytes with gold nanoparticles to track their recruitment in atherosclerosis with computed tomography. *Biomaterials* **2016**, *87*, 93–103. [CrossRef]
3. Chithrani, B.D.; Ghazani, A.A.; Chan, W.C. Determining the size and shape dependence of gold nanoparticle uptake into mammalian cells. *Nano Lett.* **2006**, *6*, 662–668. [CrossRef]
4. Kircher, M.F.; Willmann, J.K. Molecular body imaging: MR imaging, CT, and US. part I. principles. *Radiology* **2012**, *263*, 633–643. [CrossRef] [PubMed]
5. Bernstein, A.L.; Dhanantwari, A.; Jurcova, M.; Cheheltani, R.; Naha, P.C.; Ivanc, T.; Shefer, E.; Cormode, D.P. Improved sensitivity of computed tomography towards iodine and gold nanoparticle contrast agents via iterative reconstruction methods. *Sci. Rep.* **2016**, *6*, 26177. [CrossRef] [PubMed]
6. Kalishwaralal, K.; Luboshits, G.; Firer, M. Synthesis of gold nanoparticle: Peptide–drug conjugates for targeted drug delivery. In *Drug Delivery Systems*; Springer: Cham, Switzerland, 2020; pp. 145–154.
7. Rabeea, M.A.; Owaid, M.N.; Aziz, A.A.; Jameel, M.S.; Dheyab, M.A. Mycosynthesis of gold nanoparticles using the extract of Flammulina velutipes, Physalacriaceae, and their efficacy for decolorization of methylene blue. *J. Environ. Chem. Eng.* **2020**, *8*, 103841. [CrossRef]
8. Dheyab, M.A.; Aziz, A.A.; Jameel, M.S.; Khaniabadi, P.M.; Mehrdel, B.; Khaniabadi, B.M. Gold-coated iron oxide nanoparticles as a potential photothermal therapy agent to enhance eradication of breast cancer cells. *J. Phys. Conf. Ser.* **2020**, *1497*, 012003. [CrossRef]
9. Dheyab, M.A.; Owaid, M.N.; Rabeea, M.A.; Aziz, A.A.; Jameel, M.S. Mycosynthesis of gold nanoparticles by the Portabello mushroom extract, Agaricaceae, and their efficacy for decolorization of Azo dye. *Environ. Nanotechnol. Monit. Manag.* **2020**, *14*, 100312.
10. Othman, N.; Khaniabadi, P.M.; Jameel, M.S.; Dheyab, M.A.; Amiri, I. Identifying metal nanoparticle size effect on sensing common human plasma protein by counting the sensitivity of optical absorption spectra damping. *Plasmonics* **2019**, *7*, 1–11.
11. Guo, Y.; Jiang, N.; Zhang, L.; Yin, M. Green synthesis of gold nanoparticles from Fritillaria cirrhosa and its anti-diabetic activity on Streptozotocin induced rats. *Arab. J. Chem.* **2020**. [CrossRef]
12. Naharuddin, N.Z.A.; Sadrolhosseini, A.R.; Bakar, M.H.A.; Tamchek, N.; Mahdi, M.A. Laser ablation synthesis of gold nanoparticles in tetrahydrofuran. *Opt. Mater. Express* **2020**, *10*, 323–331. [CrossRef]
13. De Sousa, M.E.; van Raap, M.B.F.; Rivas, P.C.; Zelis, P.M.; Girardin, P.; Pasquevich, G.A.; Alessandrini, J.L.; Muraca, D.; Sánchez, F.H. Stability and relaxation mechanisms of citric acid coated magnetite nanoparticles for magnetic hyperthermia. *J. Phys. Chem. C* **2013**, *117*, 5436–5445. [CrossRef]
14. Quevedo, I.R.; Tufenkji, N. Influence of solution chemistry on the deposition and detachment kinetics of a CdTe quantum dot examined using a quartz crystal microbalance. *Environ. Sci. Technol.* **2009**, *43*, 3176–3182. [CrossRef]
15. Wiesner, M.R.; Lowry, G.V.; Jones, K.L.; Hochella, J.; F, M.; di Giulio, R.T.; Casman, E.; Bernhardt, E.S. Decreasing uncertainties in assessing environmental exposure, risk, and ecological implications of nanomaterials. *Environ. Sci. Technol.* **2009**. [CrossRef] [PubMed]
16. Ojea-Jiménez, I.; Puntes, V. Instability of cationic gold nanoparticle bioconjugates: The role of citrate ions. *J. Am. Chem. Soc.* **2009**, *131*, 13320–13327. [CrossRef] [PubMed]
17. Liu, J.; Aruguete, D.M.; Murayama, M.; Hochella, M.F., Jr. Influence of size and aggregation on the reactivity of an environmentally and industrially relevant nanomaterial (PbS). *Environ. Sci. Technol.* **2009**, *43*, 8178–8183. [CrossRef] [PubMed]
18. Adams, L.K.; Lyon, D.Y.; Alvarez, P.J. Comparative eco-toxicity of nanoscale TiO_2, SiO_2, and ZnO water suspensions. *Water Res.* **2006**, *40*, 3527–3532. [CrossRef] [PubMed]
19. Dederichs, T.; Moöller, M.; Weichold, O. Temperature-dependent colloidal stability of hydrophobic nanoparticles caused by surfactant adsorption/desorption and depletion flocculation. *Langmuir* **2009**, *25*, 10501–10506. [CrossRef]
20. Radziuk, D.; Grigoriev, D.; Zhang, W.; Su, D.; Moöhwald, H.; Shchukin, D. Ultrasound-assisted fusion of preformed gold nanoparticles. *J. Phys. Chem.* **2010**, *114*, 1835–1843. [CrossRef]

21. Basarir, F.; Yoon, T.-H. Sonication-assisted layer-by-layer deposition of gold nanoparticles for highly conductive gold patterns. *Ultrason. Sonochem.* **2012**, *19*, 621–626. [CrossRef]
22. Belova, V.; Moöhwald, H.; Shchukin, D.G. Sonochemical intercalation of preformed gold nanoparticles into multilayered clays. *Langmuir* **2008**, *24*, 9747–9753. [CrossRef]
23. Okitsu, K.; Ashokkumar, M.; Grieser, F. Sonochemical synthesis of gold nanoparticles: Effects of ultrasound frequency. *J. Phys. Chem. B* **2005**, *109*, 20673–20675. [CrossRef] [PubMed]
24. Takahashi, F.; Yamamoto, N.; Todoriki, M.; Jin, J. Sonochemical preparation of gold nanoparticles for sensitive colorimetric determination of nereistoxin insecticides in environmental samples. *Talanta* **2018**, *188*, 651–657. [CrossRef] [PubMed]
25. Bahrani, S.; Razmi, Z.; Ghaedi, M.; Asfaram, A.; Javadian, H. Ultrasound-accelerated synthesis of gold nanoparticles modified choline chloride functionalized graphene oxide as a novel sensitive bioelectrochemical sensor: Optimized meloxicam detection using CCD-RSM design and application for human plasma sample. *Ultrason. Sonochem.* **2018**, *42*, 776–786. [CrossRef] [PubMed]
26. Lee, J.-H.; Choi, S.U.; Jang, S.P.; Lee, S.Y. Production of aqueous spherical gold nanoparticles using conventional ultrasonic bath. *Nanoscale Res. Lett.* **2012**, *7*, 420. [CrossRef] [PubMed]
27. Zhang, J.; Du, J.; Han, B.; Liu, Z.; Jiang, T.; Zhang, Z. Sonochemical formation of single-crystalline gold nanobelts. *Angew. Chem. Int. Ed.* **2006**, *45*, 1116–1119. [CrossRef] [PubMed]
28. Usman, A.I.; Aziz, A.A.; Noqta, O.A. Green sonochemical synthesis of gold nanoparticles using palm oil leaves extracts. *Mater. Today Proc.* **2019**, *7*, 803–807. [CrossRef]
29. Usman, A.I.; Aziz, A.A.; Sodipo, B.K. Application of central composite design for optimization of biosynthesized gold nanoparticles via sonochemical method. *SN Appl. Sci.* **2019**, *1*, 403. [CrossRef]
30. Dobaradaran, S.; Nodehi, R.N.; Yaghmaeian, K.; Jaafari, J.; Niari, M.H.; Bharti, A.K.; Agarwal, S.; Gupta, V.K.; Azari, A.; Shariatifar, N. Catalytic decomposition of 2-chlorophenol using an ultrasonic-assisted Fe_3O_4–TiO_2@ MWCNT system: Influence factors, pathway and mechanism study. *J. Colloid Interface Sci.* **2018**, *512*, 172–189. [CrossRef]
31. Jameel, M.S.; Aziz, A.A.; Dheyab, M.A. Comparative analysis of platinum nanoparticles synthesized using sonochemical-assisted and conventional green methods. *Nano Struct. Nano Objects* **2020**, *23*, 100484. [CrossRef]
32. Dheyab, M.A.; Aziz, A.A.; Jameel, M.S. Synthesis and Optimization of the Sonochemical Method for Functionalizing Gold Shell on Fe_3O_4 Core Nanoparticles using Response Surface Methodology. *Surf. Interfaces* **2020**, *21*, 100647. [CrossRef]
33. Dheyab, M.A.; Aziz, A.A.; Jameel, M.S.; Noqta, O.A.; Mehrdel, B. Synthesis and coating methods of biocompatible iron oxide/gold nanoparticle and nanocomposite for biomedical applications. *Chin. J. Phys.* **2020**, *64*, 305–325. [CrossRef]
34. Fernandes, J.P.d.S.; Carvalho, B.S.; Luchez, C.V.; Politi, M.J.; Brandt, C.A. Optimization of the ultrasound-assisted synthesis of allyl 1-naphthyl ether using response surface methodology. *Ultrason. Sonochem.* **2011**, *18*, 489–493. [CrossRef]
35. Fuentes-García, J.; Santoyo-Salzar, J.; Rangel-Cortes, E.; Goya, G.; Cardozo-Mata, V.; Pescador-Rojas, J. Effect of ultrasonic irradiation power on sonochemical synthesis of gold nanoparticles. *Ultrason. Sonochem.* **2020**, *70*, 105274. [CrossRef] [PubMed]
36. Jameel, M.S.; Aziz, A.A.; Dheyab, M.A.; Mehrdel, B.; Khaniabadi, P.M. Rapid sonochemically-assisted green synthesis of highly stable and biocompatible platinum nanoparticles. *Surf. Interfaces* **2020**, *20*, 100635. [CrossRef]
37. Kim, H.-M.; Lee, C.-H.; Kim, B. Sonochemical synthesis of silica particles and their size control. *Appl. Surf. Sci.* **2016**, *380*, 305–308. [CrossRef]
38. Park, H.S.; Choi, B.G.; Yang, S.H.; Shin, W.H.; Kang, J.K.; Jung, D.; Hong, W.H. Ionic-Liquid-Assisted Sonochemical Synthesis of Carbon-Nanotube-Based Nanohybrids: Control in the Structures and Interfacial Characteristics. *Small* **2009**, *5*, 1754–1760. [CrossRef] [PubMed]
39. Okitsu, K.; Nishimura, R. Sonochemical reduction method for controlled synthesis of metal nanoparticles in aqueous solutions. In Proceedings of the 20th International Congress on Acoustics, ICA, Sydney, Australia, 23–27 August 2010.
40. Wang, A.; Ng, H.P.; Xu, Y.; Li, Y.; Zheng, Y.; Yu, J.; Han, F.; Peng, F.; Fu, L. Gold nanoparticles: Synthesis, stability test, and application for the rice growth. *J. Nanomater.* **2014**, *2014*. [CrossRef]

41. Piella, J.; Bastús, N.G.; Puntes, V. Size-Controlled Synthesis of Sub-10-nanometer Citrate-Stabilized Gold Nanoparticles and Related Optical Properties. *Chem. Mater.* **2016**, *28*, 1066–1075. [CrossRef]
42. Dong, Y.C.; Hajfathalian, M.; Maidment, P.S.; Hsu, J.C.; Naha, P.C.; Si-Mohamed, S.; Breuilly, M.; Kim, J.; Chhour, P.; Douek, P. Effect of gold nanoparticle size on their properties as contrast agents for computed tomography. *Sci. Rep.* **2019**, *9*, 1–13. [CrossRef]
43. Peng, C.; Li, K.; Cao, X.; Xiao, T.; Hou, W.; Zheng, L.; Guo, R.; Shen, M.; Zhang, G.; Shi, X. Facile formation of dendrimer-stabilized gold nanoparticles modified with diatrizoic acid for enhanced computed tomography imaging applications. *Nanoscale* **2012**, *4*, 6768–6778. [CrossRef]
44. Sodipo, B.K.; Aziz, A.A. One minute synthesis of amino-silane functionalized superparamagnetic iron oxide nanoparticles by sonochemical method. *Ultrason. Sonochem.* **2018**, *40*, 837–840. [CrossRef] [PubMed]
45. Rayathulhan, R.; Sodipo, B.K.; Aziz, A.A. Nucleation and growth of zinc oxide nanorods directly on metal wire by sonochemical method. *Ultrason. Sonochem.* **2017**, *35*, 270–275. [CrossRef] [PubMed]
46. Bai, R.G.; Muthoosamy, K.; Zhou, M.; Ashokkumar, M.; Huang, N.M.; Manickam, S. Sonochemical and sustainable synthesis of graphene-gold (G-Au) nanocomposites for enzymeless and selective electrochemical detection of nitric oxide. *Biosens. Bioelectron.* **2017**, *87*, 622–629.
47. Prasad, R.; Dalvi, S.V. Sonocrystallization: Monitoring and controlling crystallization using ultrasound. *Chem. Eng. Sci.* **2020**, 115911. [CrossRef]
48. Robinson, I.; Tung, L.D.; Maenosono, S.; Wälti, C.; Thanh, N.T. Synthesis of core-shell gold coated magnetic nanoparticles and their interaction with thiolated DNA. *Nanoscale* **2010**, *2*, 2624–2630. [CrossRef]
49. Ilgin, P.; Ozay, O.; Ozay, H. A novel hydrogel containing thioether group as selective support material for preparation of gold nanoparticles: Synthesis and catalytic applications. *Appl. Catal. B* **2019**, *241*, 415–423. [CrossRef]
50. Sahoo, P.K.; Wang, D.; Schaaf, P. Tunable plasmon resonance of semi-spherical nanoporous gold nanoparticles. *Mater. Res. Express* **2014**, *1*, 035018. [CrossRef]
51. Zhou, H.; Lee, J.; Park, T.J.; Lee, S.J.; Park, J.Y.; Lee, J. Ultrasensitive DNA monitoring by Au–Fe_3O_4 nanocomplex. *Sens. Actuators B* **2012**, *163*, 224–232. [CrossRef]
52. Karamipour, S.; Sadjadi, M.; Farhadyar, N. Fabrication and spectroscopic studies of folic acid-conjugated Fe_3O_4@ Au core–shell for targeted drug delivery application. *Spectrochim. Acta Part A* **2015**, *148*, 146–155. [CrossRef]
53. Kim, H.N.; Suslick, K.S. The effects of ultrasound on crystals: Sonocrystallization and sonofragmentation. *Crystals* **2018**, *8*, 280. [CrossRef]
54. Daniel, M.-C.; Astruc, D. Gold nanoparticles: Assembly, supramolecular chemistry, quantum-size-related properties, and applications toward biology, catalysis, and nanotechnology. *Chem. Rev.* **2004**, *104*, 293–346. [CrossRef]
55. Link, S.; El-Sayed, M.A. Size and temperature dependence of the plasmon absorption of colloidal gold nanoparticles. *J. Phys. Chem. B* **1999**, *103*, 4212–4217. [CrossRef]
56. Paul, K.G.; Frigo, T.B.; Groman, J.Y.; Groman, E.V. Synthesis of ultrasmall superparamagnetic iron oxides using reduced polysaccharides. *Bioconjugate Chem.* **2004**, *15*, 394–401. [CrossRef]
57. Dheyab, M.A.; Aziz, A.A.; Jameel, M.S.; Noqta, O.A.; Khaniabadi, P.M.; Mehrdel, B. Simple rapid stabilization method through citric acid modification for magnetite nanoparticles. *Sci. Rep.* **2020**, *10*, 10793. [CrossRef]
58. Kumar, A.; Dixit, C.K. Methods for characterization of nanoparticles. In *Advances in Nanomedicine for the Delivery of Therapeutic Nucleic Acids*; Elsevier: Potsdam, NY, USA, 2017; pp. 43–58.
59. Bagheri, S.; Aghaei, H.; Ghaedi, M.; Asfaram, A.; Monajemi, M.; Bazrafshan, A.A. Synthesis of nanocomposites of iron oxide/gold (Fe_3O_4/Au) loaded on activated carbon and their application in water treatment by using sonochemistry: Optimization study. *Ultrason. Sonochem.* **2018**, *41*, 279–287. [CrossRef] [PubMed]
60. Sana, S.; Boodhoo, K.; Zivkovic, V. Production of starch nanoparticles through solvent-antisolvent precipitation in a spinning disc reactor. *Green Process. Synth.* **2019**, *8*, 507–515. [CrossRef]
61. Souza, T.G.; Ciminelli, V.S.; Mohallem, N.D.S. A comparison of TEM and DLS methods to characterize size distribution of ceramic nanoparticles. *J. Phys. Conf. Ser.* **2016**, *733*, 6–11. [CrossRef]
62. Hagendorfer, H.; Kaegi, R.; Parlinska, M.; Sinnet, B.; Ludwig, C.; Ulrich, A. Characterization of silver nanoparticle products using asymmetric flow field flow fractionation with a multidetector approach—A comparison to transmission electron microscopy and batch dynamic light scattering. *Anal. Chem.* **2012**, *84*, 2678–2685. [CrossRef]

63. Yang, L.; Kuang, H.; Zhang, W.; Aguilar, Z.P.; Wei, H.; Xu, H. Comparisons of the biodistribution and toxicological examinations after repeated intravenous administration of silver and gold nanoparticles in mice. *Sci. Rep.* **2017**, *7*, 1–12. [CrossRef]
64. Labouta, H.I.; Sarsons, C.; Kennard, J.; Gomez-Garcia, M.J.; Villar, K.; Lee, H.; Cramb, D.T.; Rinker, K.D. Understanding and improving assays for cytotoxicity of nanoparticles: What really matters? *RSC Adv.* **2018**, *8*, 23027–23039. [CrossRef]
65. Mahmoudi, M.; Simchi, A.; Milani, A.; Stroeve, P. Cell toxicity of superparamagnetic iron oxide nanoparticles. *J. Colloid Interface Sci.* **2009**, *336*, 510–518. [CrossRef] [PubMed]
66. Zhao, H.Y.; Liu, S.; He, J.; Pan, C.C.; Li, H.; Zhou, Z.Y.; Ding, Y.; Huo, D.; Hu, Y. Synthesis and application of strawberry-like Fe_3O_4-Au nanoparticles as CT-MR dual-modality contrast agents in accurate detection of the progressive liver disease. *Biomaterials* **2015**, *51*, 194–207. [CrossRef] [PubMed]
67. Wu, W.; Hao, R.; Liu, F.; Su, X.; Hou, Y. Single-crystalline α-Fe_2O_3 nanostructures: Controlled synthesis and high-index plane-enhanced photodegradation by visible light. *J. Mater. Chem. A* **2013**, *1*, 6888–6894. [CrossRef]
68. Hu, Y.; Li, J.-C.; Shen, M.-W.; Shi, X.-Y. Formation of multifunctional Fe3O4/Au composite nanoparticles for dual-mode MR/CT imaging applications. *Chin. Phys. B* **2014**, *23*, 078704. [CrossRef]
69. Popovtzer, R.; Agrawal, A.; Kotov, N.A.; Popovtzer, A.; Balter, J.; Carey, T.E.; Kopelman, R. Targeted gold nanoparticles enable molecular CT imaging of cancer. *Nano Lett.* **2008**, *8*, 4593–4596. [CrossRef]
70. Ajeesh, M.; Francis, B.; Annie, J.; Varma, P.H. Nano iron oxide–hydroxyapatite composite ceramics with enhanced radiopacity. *J. Mater. Sci. Mater. Med.* **2010**, *21*, 1427–1434. [CrossRef]
71. Li, J.; Zheng, L.; Cai, H.; Sun, W.; Shen, M.; Zhang, G.; Shi, X. Facile one-pot synthesis of Fe_3O_4@ Au composite nanoparticles for dual-mode MR/CT imaging applications. *ACS Appl. Mater. Interfaces* **2013**, *5*, 10357–10366. [CrossRef]
72. Xu, C.; Tung, G.A.; Sun, S. Size and concentration effect of gold nanoparticles on X-ray attenuation as measured on computed tomography. *Chem. Mater.* **2008**, *20*, 4167–4169. [CrossRef]